Desalination and Water Treatment
www.deswater.com

doi: 10.5004/dwt.2021.27261

226 (2021) 303–318
June

Facile fabrication of a novel silico vanadate ion exchanger: evaluation of its sorption behavior towards europium and terbium ions

E.A. Abdel-Galil*, A.B. Ibrahim, W.M. El-Kenany

Hot Laboratories and Waste Management Center, Egyptian Atomic Energy Authority, 13759 Cairo, Egypt, Tel. +20 1159895618/ +20 1281294400; Fax: 20 244620784; email: ezzat_20010@yahoo.com (E.A. Abdel-Galil), Tel. +20 1009327167; Fax: 20 244620784; email: Asmaabendary80@yahoo.com (A.B. Ibrahim), Tel. +20 1220591122; Fax: 20 244620784; email: wafaamohamed4312@yahoo.com (W.M. El-Kenany)

Received 7 November 2020; Accepted 21 March 2021

ABSTRACT

A novel inorganic silico vanadate (SiV) was synthesized via a sol–gel technique. The granulometry, morphology, and structure of the prepared exchanger were studied using different analytical tools such as X-ray fluorescence, Fourier-transform infrared, scanning electron microscopy, X-ray diffraction, transmission electron microscopy, and thermogravimetric analysis–differential thermal analysis. The structure of SiV exchanger may be composed as $(H_2V_2O_8)(HSiO_2)_2{\cdot}1.5H_2O$. Batch tests were done to examine the sorption behavior of SiV towards Eu(III) and Tb(III) considering the influence of independent parameters including pH of the solution, contact time, sorbent weight, and initial metal ions concentration. The sorption efficiency values of 95.40% and 88.70% were respectively obtained for Eu(III) and Tb(III) at optimum conditions (pH = 5.5, C_0 = 50 mg/L, weight = 0.03 g, and time = 200 min). The equilibrium data fitted well to the non-linear Freundlich and Langmuir isotherm models and the maximum adsorption capacity (q_m) of SiV for Eu(III) and Tb(III) get from the non-linear Langmuir model was 44.23 and 34.39 mg/g, respectively. Kinetic studies showed that the sorption of Eu(III) and Tb(III) followed both pseudo-second-order and intraparticle diffusion models. The thermodynamic studies showed an endothermic and spontaneous sorption process. The sorbent material can also be reactivated by utilizing the solution of 0.4 mol/L HNO_3 and re-used again effectively.

Keywords: Inorganic ion-exchanger; Silico vanadate; Sorption; Europium; Terbium; Decontamination factor; Isotherm; Kinetic; Thermodynamic; Liquid radioactive waste

1. Introduction

Rare earth metals (REMs) are turning out to be progressively significant because of their unique chemical and physical properties and their applications in the field of compound designing, metallurgy, nuclear energy, optical, magnetic, luminescence, and laser materials, high-temperature superconductors, and secondary batteries, etc [1,2]. REMs for the most part fall into two classes, viz. light rare earth metals and heavy rare earth metals, with changing degrees of employments and request. Light rare earth metals include lanthanum (La), cerium (Ce), praseodymium (Pr), neodymium (Nd), samarium (Sm) and heavy rare earths include europium (Eu), gadolinium (Gd), terbium (Tb), dysprosium (Dy), holmium (Ho), erbium (Er), thulium (Tm), ytterbium (Yb), lutetium (Lu), yttrium (Y) which are less common and more significant [3].

Terbium is a special element since it is needed to make cathode ray tubes, optical computers, and various alloys [4]. Terbium offers radioisotopes suitable for PET, SPECT diagnosis, and α and β^- therapy as well. ^{155}Tb seems to be an ideal nuclide for diagnostic imaging [5]. Its half-life of

* Corresponding author.

5.3 d is long enough to observe even slower metabolic processes. The characteristic γ-rays at 87 and 105 keV are ideal for most SPECT cameras. ^{152g}Tb seems to be promising for quantitative imaging with PET [6]. The positron intensity of 17% and the mean positron energy of 1.1 MeV are suitable. For targeted particle therapy both the ^{149}Tb ($T_{1/2}$ = 4.1 h, I_α = 17%) and ^{161}Tb ($T_{1/2}$ = 6.9 d, I_β = 100%) seems to be promising [7]. These isotopes can be formed with particle accelerator [5,6,8–10] or in nuclear reactors [7,11] depending on which isotope is necessary for the given application.

Europium represents in the medical field as a new paramagnetic agent in the magnetic resonance imaging domain [12]. It is also used on various clinical diagnoses to determine some renal and cardiac diseases [12,13], as a test to determine the blood hormone levels [14]. $^{152+154}$Eu isotopes are produced primarily as fission products [15]. It can also be produced by neutron activation of nuclear reactor control rods [16]. Therefore, it is found in certain places, around nuclear reactors and facilities that process spent nuclear fuel. Europium-154 ($T_{1/2}$ = 8.592 y) emits multiple γ-photons and is a co-produced radionuclide during the formation of ^{153}Sm [17] as described below:

$$^{152}\text{Sm}\ (n,\gamma)\ ^{153}\text{Sm}\ (\beta^-,46{:}284\ \text{h}) \rightarrow\ ^{153}\text{Eu}\ (n,\gamma)\ ^{154}\text{Eu}$$

Therefore, it has become necessary to develop a suitable technology for the recovery of rare earth metals. Various techniques have been proposed for the recovery of REMs, for example, co-precipitation, solvent extraction, ion-exchange, solid-phase extraction, etc [18–22]. Solvent extraction and ion-exchange are the two most common methodologies for the recovery of REMs from various matrices. Solvent extraction is inefficient because of the requirement of a large volume of solvent, which may create health problems [23]. The researchers directed their interest in using the ion exchange technique for the recovery of REMs. Synthetic inorganic ion-exchanger has been used more extensively in the past two decades owing to their thermal stability at elevated temperatures, resistance to high radiation fields, and their selectivity to certain ions [24]. The selectivity and ion-exchange properties of a material depend considerably on its chemical composition. It is, therefore, always interesting to synthesize new materials and to study their ion-exchange behavior [24]. In addition, various attempts have been made to examine the cation sorption behavior of insoluble solids. In the case of our systematic studies on inorganic ion-exchangers, we found that silico vanadate (SiV) has a selective behavior for Eu(III) and Tb(III) ions. The few studies on the vanadates as ion-exchangers have been summed up as of late.

The current paper is concerned with the synthesis of SiV as an inorganic ion exchanger via the sol–gel method. Physicochemical properties of this ion exchange material were determined utilizing some instrumental examinations viz. Fourier-transform infrared spectroscopy (FT-IR), X-ray diffraction (XRD), thermogravimetric analysis (TGA), differential thermal analysis (DTA), scanning electron microscopy (SEM), transmission electron microscopy (TEM), and elemental analysis. Its sorption ability was considered for Eu(III) and Tb(III) removal from aqueous solutions using the batch sorption method. Some factors influencing sorption, for example, contact time, initial pH of the solution, sorbent weight, as well as initial concentration of Eu(III) and Tb(III), were examined. Kinetic and isotherm sorption tests were studied. Thermodynamic parameters for sorption of Eu(III) and Tb(III) ions were determined. Adsorption, desorption, and regeneration studies of SiV were likewise done.

2. Experimental

2.1. Reagents and chemicals

The main reagents used for the synthesis of inorganic silico vanadate (SiV) were sodium metasilicate ($Na_2O_3Si{\cdot}9H_2O$) and sodium metavanadate ($NaVO_3$) and were obtained from Loba Chemie (India). Chemicals such as HCl, europium(III) chloride hexahydrate ($EuCl_3{\cdot}6H_2O$), and terbium(III) chloride hexahydrate ($TbCl_3{\cdot}6H_2O$) were bought from Merck (Germany) as analytical-grade reagents, and double-distilled water (DDW) was used. Other reagents and synthetic substances were of analytical grade. Measurements of the initial pH of Eu(III) and Tb(III) ions solutions were done utilizing a lab pH-meter, model pH 601A (USA). A preliminary calibration is systematically carried out using suitable buffer solutions.

2.2. Radioisotopes

Radioisotopes $^{152+154}$Eu and ^{160}Tb have been obtained by neutron activation of their metal chloride salts in front of the neutron flux produced in the core of the Egyptian second research reactor (ETRR-II). The activated salts have been dissolved in DDW to form the aqueous solution considering the radiation protection rules.

2.3. Radiometric assay

The radionuclides of $^{152+154}$Eu and ^{160}Tb have been assessed by measuring their emitted γ-rays using a high resolution P-type coaxial High Purity Germanium Detector HPGe-GX2518 Model, Canberra, USA, with lead shield casing. The HPGe detector is coupled with a multi-channel analyzer having 16,384 channels ADC, power supply, and amplifier in one unit (Inspector, 2000 Model, Canberra Series, USA).

2.4. Synthesis of silico vanadate

Fabrication of SiV exchanger was achieved by adding 0.5 mol/L sodium metasilicate into 0.5 mol/L sodium metavanadate by volume/volume ratio of 1:1 on a magnetic stirrer with constant stirring at 25°C ± 1°C for 1 h. The pH of the mixture solution was estimated and discovered to be 11.70. The pH was adjusted to be 0.75 by adding HCl. The color of the mixture converted from colorless to dark orange color and the orange precipitate was formed. The obtained orange-colored precipitate was kept for digestion with mother liquor for 24 h. After 24 h the supernatant liquid was decanted off and the precipitate was filtered and washed several times with DDW to remove

unreacted impurities. The precipitate was dried in an oven at 50°C ± 1°C, after that, it was broken into small size granules, and was converted into H^+ form by treating with 0.1 mol/L HNO_3 for 24 h. Finally, the product was filtered out and washed with DDW several times to remove the excess acid and oven-dried at 50°C ± 1°C. The color of the dried granules became dark brown. The detailed conditions for synthesis were given in Table 1.

2.5. Instruments

The elemental analysis of the prepared SiV has been investigated utilizing the X-ray fluorescence spectrometry, XRF-2400 (Philips, Holland). The FT-IR of SiV was recorded using a BOMEM-FTIR spectrophotometer (Shimadzu, Kyoto, Japan) and recorded in the scope of 400–4,000 cm^{-1}. Physical properties such as morphology shape and size distribution of the sample were characterized by utilizing the JSM-6510A SEM (Japan) and JEOL JEM-100cx TEM (Japan). The XRD patterns of the samples were observed by an XD–Dl (Shimadzu, Kyoto, Japan) and carried out at 30 kV, 30 mA, and a diffraction angle (2θ) range of 4°–90°. TGA and DTA were completed at a heating rate of 10°C/min using a DTG-60/60H thermal analyzer (Shimadzu, Kyoto, Japan).

2.6. pH titration studies

Topp and Pepper method was utilized for pH titration considers [25]. 0.1 g of the SiV exchanger was taken in each of several conical flasks followed by equimolar solutions of alkali metal chlorides and their hydroxides in different volume ratios, the final volume being 10 mL to maintain the ionic strength constant (0.1 mol/L). The pH of the solution was recorded every 24 h until equilibrium was achieved. The pH at equilibrium was plotted against the millimoles of OH^- ions added.

2.7. Chemical stability

One hundred milligrams portions of the prepared SiV in H^+ form were treated with 100 mL each of different acids like HCl, HNO_3, H_2SO_4, and different bases such as NaOH, KOH, organic solvents such as acetone, n-butyl alcohol, and also with DDW for 48 h with occasional shaking at room temperature. The quantity of exchanger material released into the solution was determined gravimetrically.

2.8. Ion-exchange capacity and thermal effect

To decide the impact of heating temperature on ion-exchange capacity (IEC), 1 g sample of the prepared material was heated at various temperatures (50°C, 100°C, 200°C, 300°C, 400°C, 500°C, and 600°C ± 2°C) in a muffle furnace for 4 h and Eu^{3+} ion-exchange capacity was determined after cooling them at room temperature using the batch technique by mixing 0.1 g of previously heated SiV with 10 mL Eu(III) ion solution (100 mg/L) at V/m = 100 mL/g. The mixture was continuously shaken in a thermostatic water bath shaker (Kottermann D-1362, Germany) at 200 rpm for 24 h till equilibration was attained. After equilibrium, the solution was filtered and the concentration of Eu(III) ions was measured using an inductively coupled plasma-atomic emission spectrometer (ICP-AES) device, (ICPs-7500) manufactured and supplied by Shimadzu (Kyoto, Japan). This procedure was repeated many times with new Eu(III) ion solutions or until the SiV was saturated with Eu(III) ions. The value of capacity (mg/g) was determined by the next equation:

$$\text{Capacity (mg/g)} = \frac{C_0 - C_f}{m} \times V \quad (1)$$

where C_0 and C_f are the concentrations of the ions in solution before and after equilibrium (mg/L), respectively, V is the solution volume (L) and m is the sorbent mass (g).

2.9. Batch sorption experiment

Sorption of Eu(III) and Tb(III) onto SiV was studied by batch experiments. A known amount of the above-mentioned metal ions solutions (50–500 mg/L) was taken with 30 mg of SiV in the 10 mL penicillin tubes which were sealed and agitated (V/m = 100 mL/g) at 200 rpm in a thermostatic water bath shaker (Kottermann D-1362, Germany). The pH of the adsorbate solution was adjusted with 0.1 mol/L HCl solutions. The trial penicillin tubes were withdrawn at a predetermined time interval until the sorption equilibrium was accomplished. The metal ion solutions were separated by centrifugation operated at

Table 1
Conditions of synthesis of SiV exchanger

Sample	Mixing volume ratio (v/v)		Total volume (mL)	pH	Condition	Appearance of beads after drying at 50°C ± 1°C	Yield (g)	Ion-exchange capacity mg/g (Eu^{3+})
	$NaVO_3$ in DDW (0.5 mol/L)	$Na_2O_3Si{\cdot}9H_2O$ in DDW (0.5 mol/L)						
Silico vanadate (SiV)	1	1	200 mL	0.75	25°C ± 1°C	Dark brown	4.88	25.16

4,000 rpm for 5 min. The supernatants were then filtered to guarantee that solutions were liberated from SiV before measuring the remaining metal ion concentration. The staying metal ions in the filtrate were analyzed using the ICP-AES device, ICPs-7500. Different parameters for Eu(III) and Tb(III) sorption were studied including the effect of pH of the solution (1.50–5.50), contact time (5–1,440 min), initial metal ion concentration (50–500 mg/L), and sorbent weight (7.5–120 mg). All the experiments are repeated three times and then the average for the values are assigned. The total experimental percentage error did not exceed 3%. The sorption percentage and amount of metal ion sorption per unit mass of SiV at equilibrium (q_e, mg/g) were evaluated using the following mass balance equations;

$$\text{Sorption } \% = \left(\frac{C_0 - C_f}{C_0}\right) \times 100 \quad (2)$$

$$q_e(\text{mg/g}) = \frac{\left(C_0 - C_f\right)V}{m} \quad (3)$$

3. Results and discussion

3.1. Characterization of SiV

3.1.1. Chemical composition

The material was analyzed for Si(IV) and vanadate by X-ray fluorescence spectrometry (XRF). The weight % composition of the material was: SiO_2, 8.79%; V_2O_3, 84.06%; H_2O, 7.14%.

3.1.2. Fourier-transform infrared spectroscopy

The FT-IR spectroscopy was performed to determine the functional groups of SiV. The FT-IR spectra of SiV exchanger were presented in Fig. 1a. As appeared in Fig. 1a, the peaks at 510.40 and 771.85 cm^{-1} are due to Si–O–Si rocking mode and asymmetric stretching vibrations of Si–OH, respectively [26]. A smaller peak at 920.26 cm^{-1} has been assigned to a V–O–Si bond vibration [27]. The intense peak in the SiV spectrum at 1,010.22 cm^{-1} could be appointed to terminal V=O bonds [28]. The characteristic Si–O stretching band can be observed at around 1,219.82 cm^{-1} [29]. The peak at 1,401.31 cm^{-1} relates to the deformation vibration of hydroxyl groups (maybe Si and/or V–OH deformation vibration) [30]. The peak at 1,617.76 cm^{-1} has corresponded to the bending mode of water molecules [30]. The broad absorption band at 3,158.29 cm^{-1} because of the stretching vibration of the hydroxyl group [26] and the intensity of the absorption band at 3,372.52 cm^{-1} due to silanol $^{-}$OH groups [31].

Fig. 1b illustrates the FT-IR images of SiV before and after loading with Tb^{3+} and Eu^{3+} ions, respectively. These images were used as a tool to determine the structure and vibration frequency changes of the functional groups in the ion exchange material after its saturation with the studied cations. According to Fig. 1b, it could saw that the intensity of all peaks is changed and improved after loading of Tb(III) and Eu(III). These significant changes in the intensity of these peaks after loading of Tb(III) and Eu(III) indicate that H_2O, $^{-}$OH, vanadate ion, Si–O–H, and V–O–H were involved in the uptaking of Tb(III) and Eu(III).

3.1.3. Scanning electron microscopy

SEM photograph of SiV (Fig. 2) shows a spherical shape with different sizes. These irregular circles are grouped forming an irregular elongated shape. This irregular morphology indicates the existence of impure phases. Thus it was confirmed from the XRD study.

3.1.4. X-ray diffractometry

XRD pattern of the prepared exchanger (Fig. 3) shows low intense peaks at different 2θ values. The patterns

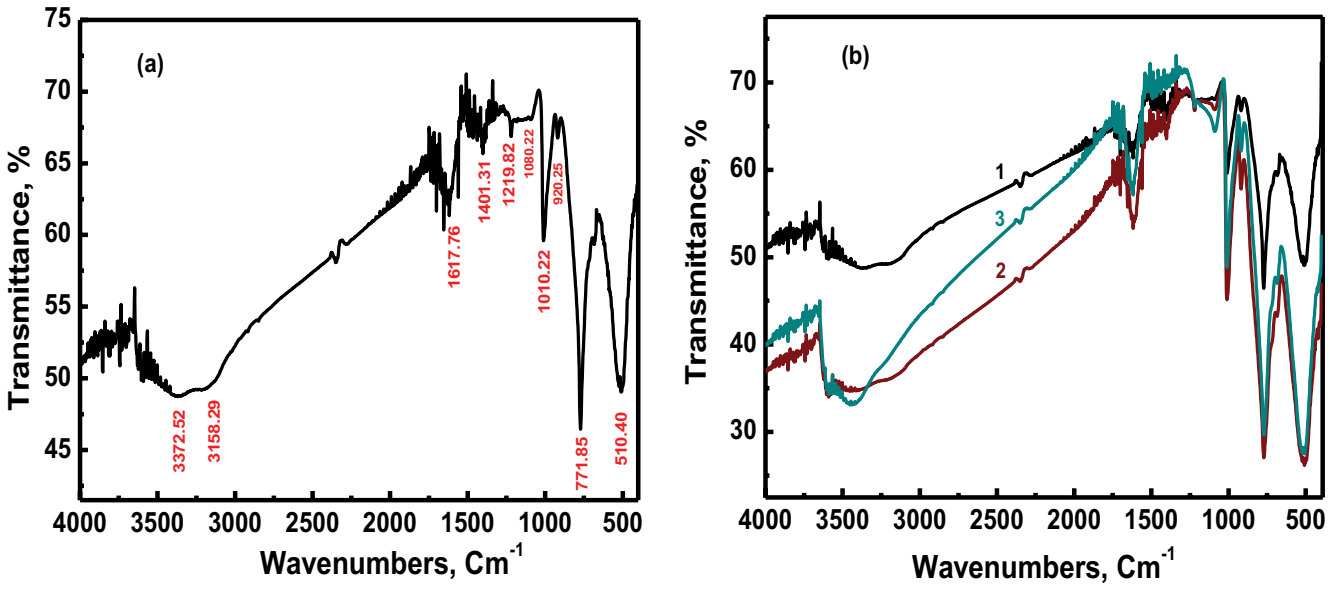

Fig. 1. FT-IR spectrum of (a) SiV and (b) [(1) unloaded SiV; (2) Tb(III)-loaded SiV; (3) Eu(III)-loaded SiV].

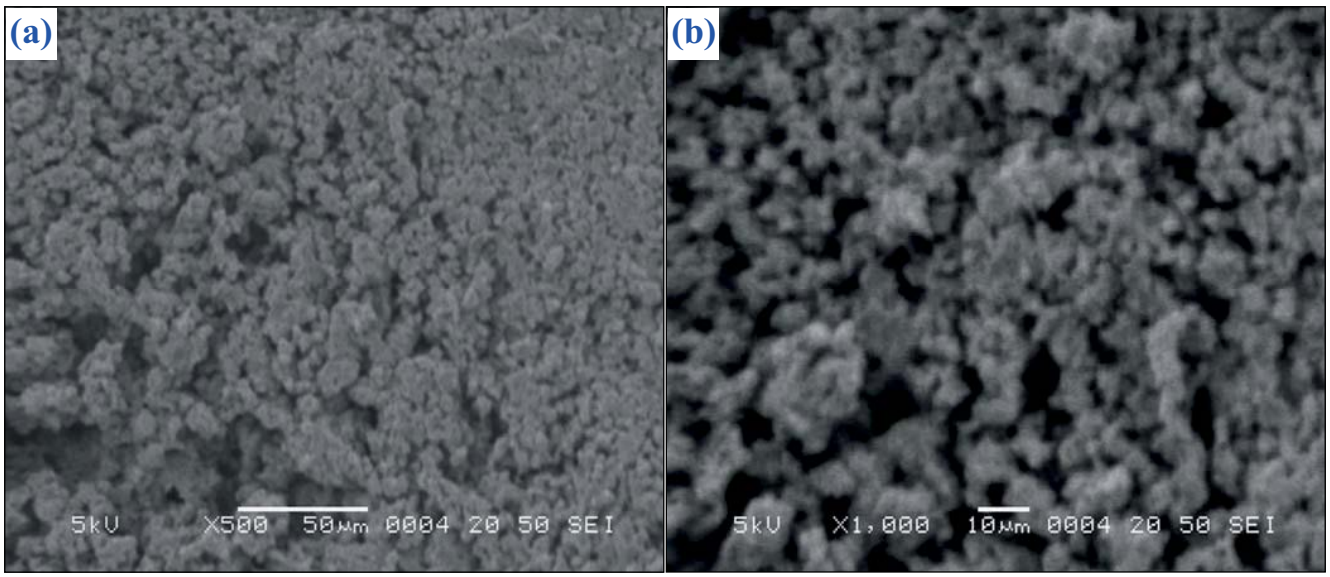

Fig. 2. SEM of SiV exchanger: (a) magnitude of 500× and (b) magnitude of 1,000×.

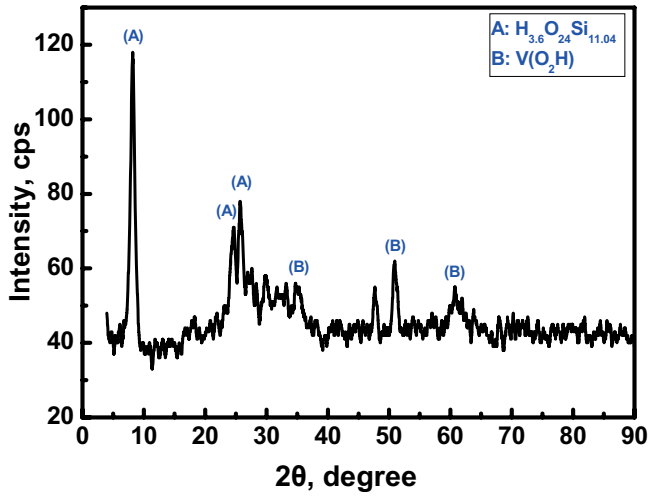

Fig. 3. XRD patterns of SiV exchanger.

confirm that SiV consisted of mixed phases [$H_{3.6}O_{24}Si_{11.04}$ and $V(O_2H)$] as seen in Table 2. The average diameter for each phase was discovered to be 10.27 and 11.17 nm respectively, which determined from the full width at half-maximum of the most intense peak at 8.17 and 50.97 degrees (2θ) for $H_{3.6}O_{24}Si_{11.04}$ and $V(O_2H)$ phases respectively, using Debye Scherrer's equation [32]:

$$D = \frac{K\lambda}{\beta\cos\theta} \quad (4)$$

where D is the crystallite size in nm, λ is the characteristic wavelength of X-ray used (CuKα = 1.541836), θ is the diffraction angle, and β is the angular width in radians at an intensity equal to half of the maximum peak intensity [33].

3.1.5. Transmission electron microscopy

The detailed structures of the prepared SiV exchanger are displayed in TEM images (Fig. 4). It can be seen that the sample has irregular shape particles confirming that more than one component agglomerate with each other, a large vanadate component is intimately mixed with nanosized silica. Nanosized black circle corresponded to silica are dispersed on the vanadate matrix which exists in a needle bundles shape. The TEM images have been used just to estimate and check-up the average size of the particles; where for the nanosized silica it is found to be 7 nm and for the bulk vanadate sample it is about 984 nm. The obtained results are compatible with the XRD ones.

3.1.6. Thermogravimetric and differential thermal analyses

TGA and DTA of SiV were conducted using a Shimadzu DTG-60/60H thermal analyzer obtained from Shimadzu (Kyoto, Japan). The sample was heated from room temperature up to 600°C ± 1°C at 10°C/min with a sample holder made of Al_2O_3 under nitrogen flow (40 mL/min), alumina powder was utilized as reference material. On the basis of the nature of TGA–DTA curves (Figs. 5a and b), the material exhibits a weight loss of 7.14 wt.% between 20°C and 114°C (at about 83.30°C), which is attributed mostly to the desorption of absorbed water [34–36]. During heating from 115°C to 320°C (at about 144.61°C), the sample loses additional 6.24 wt.% water that can be credited to the removal of interstitial water molecules by condensation of exchangeable hydroxyl groups ($^-$OH) from the material, which is characteristic of synthetic inorganic ion exchangers [35]. An exothermic peak is noticed at 333°C may be caused by physical transitions such as crystallization occurring during heating [35]. The water content for the prepared sample evaporated at about 320°C. In total, SiV lost about 13.38 wt.% of its total weight because of the water loss when heated up to 320°C [36]. There is no significant weight

Table 2
XRD data of SiV exchanger

No.	2θ	d (Å)	I/I_0	FWHM	Matched	JCPDS	D
1	8.17	10.82	100	0.7733	A	99-002-4297	10.27
2	24.54	3.62	28	0.8400	A		
3	25.75	3.46	36	0.7400	A		
4	34.85	2.57	11	0.6200	B	99-100-0071	
5	50.97	1.79	26	0.7800	B		11.18
6	60.68	1.53	17	0.400	B		

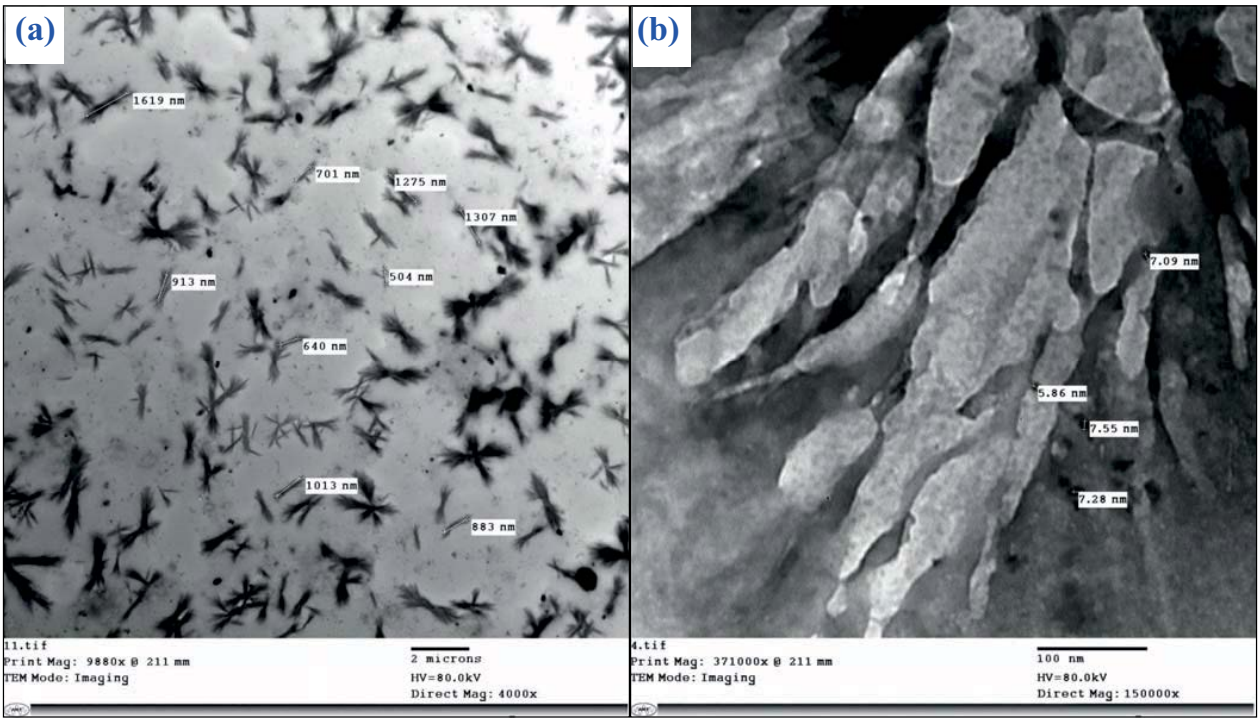

Fig. 4. (a and b) Bright-field TEM images of the prepared SiV.

reduction after 320°C which demonstrates that no structural changes occur in the material. The curve pattern suggests that the ion exchanger is stable up to 600°C. The 7.14% weight loss of mass represented by the TGA curve between 20°C and 114°C must be due to the loss of $n$$H_2O$ from the ion exchanger structure. The value of "n", the external water molecules, can be determined utilizing Alberti's equation.

$$18n = X\left[\frac{M+18n}{100}\right] \quad (5)$$

where X is the percent weight loss (7.14%) of the exchanger by heating up to 114°C and (M + 18n) is the molecular weight of the material without water molecules. The calculations give ~1.5 for the external water molecule (n) per molecule of the cation-exchanger. As a result of the above findings, a temporary formula of $(H_2V_2O_8)(HSiO_2)_2 \cdot 1.5H_2O$ has been assigned to the exchanger.

3.1.7. pH titration study

The pH titrations in the presence of SiV were performed for NaCl–NaOH systems under equilibrium conditions [26,37]. The pH titration curve (Fig. 6) shows that SiV releases H^+ ions on the addition of NaCl solution to the system, which is indicated by a pH value ~ 3.48 of the solution. Further, the titration curve shows two inflection points demonstrating that SiV exchanger behaves as a bi-functional ion exchanger. This result indicates those two functional groups are responsible for releasing its H^+ to be exchanged with the studied cations, these functional groups may be Si–O–H and V–O–H as appeared in XRD and FT-IR sections.

3.1.8. Chemical stability

The solubility experiment (Table 3) indicated that the material was very steady in common mineral acids, organic solvents, and alkalies. Table 3 shows that SiV exchanger

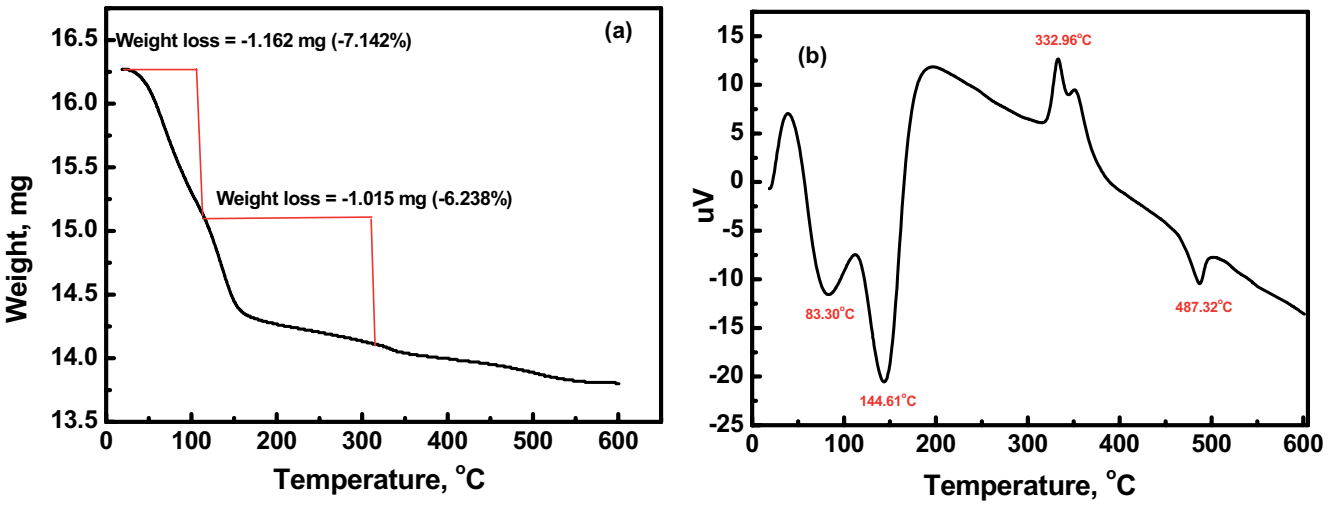

Fig. 5. (a) Thermogravimetric analysis (TGA) and (b) differential thermal analysis (DTA) of SiV exchanger.

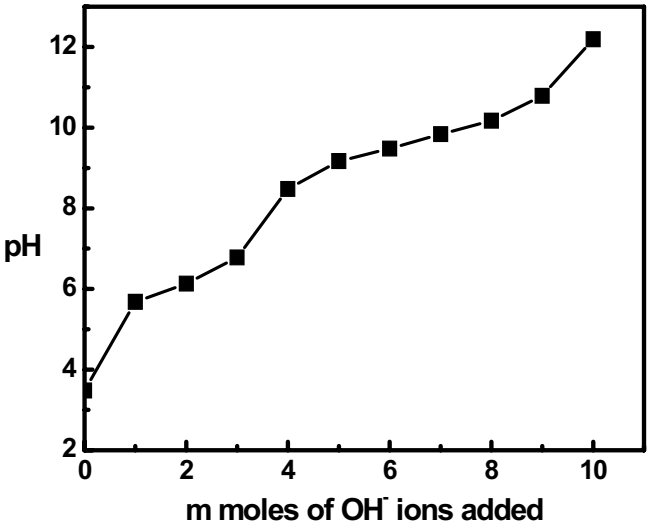

Fig. 6. pH titration curve of SiV exchanger with NaCl–NaOH system.

possesses relatively high chemical stability compared to other ion exchange materials [37–41].

3.1.9. Thermal stability

It is observed from Table 4 that on heating the prepared SiV at various temperatures for 4 h, the mass and ion-exchange capacity was changed. The material was found to have higher thermal stability as the sample maintained about 85% of the initial mass by heating up to 600°C. However, in respect to ion-exchange capacity, this material was found stable up to 600°C. Where it holds about 72% of its initial ion-exchange capacity by heating up to 600°C. The prepared SiV exchanger has high thermal stability comparing with other inorganic ion exchangers [35,37].

In order to explore the reason for decreasing the exchange capacity with the increase in the temperature. When SiV exchanger heated to an elevated temperature it lost most of its external and structural water which are responsible for exchange capacity, this was accomplished with the decrease in IEC of the prepared exchanger [35].

Table 3
Solubility of SiV exchanger in various solvent systems

Solvent	Solubility (g/L)
1 mol/L HCl	0.140
1 mol/L HNO_3	0.110
1 mol/L H_2SO_4	0.125
0.1 mol/L NaOH	0.075
0.1 mol/L KOH	0.022
Acetone	BD
n-Butanol	0.0014
DDW	BD

BD: below detection.

3.2. Batch method sorption studies

3.2.1. Effect of pH

The sorption of Eu(III) and Tb(III) ions by SiV exchanger as a function of pH was studied at temperature 25°C ± 1°C and sorbent dosage 10 g/L. In the chose range of pH (from 1.50–5.50) for this study, it was seen that the sorption of Eu(III) and Tb(III) ions by SiV increased with increasing the pH of the solutions as appears in Fig. 7. The maximum sorption was achieved at pH 5.50 and was discovered to be 95.40% and 88.70% for Eu(III) and Tb(III) ions, respectively. The lowering in the sorption percentage in high acidic solution (low pH) can be ascribed to the surface of the SiV would be closely associated with hydronium ions (H_3O^+). Similar charges in adsorbate (metals ions) and sorbent surface (because of the existence of H_3O^+ ions) were causing electrostatic repulsion and this hindered the access of metal ions to the exchanger surface. Consequently, the sorption was found to be decreased [42].

Table 4
Effect of temperature on ion-exchange capacity of SiV exchanger

Temperature (°C)	Weight loss (%)	IEC (mg/g)	% Retention of IEC
50	0.90	25.16	100
100	5.93	24.43	97.09
200	12.32	23.28	92.53
300	13.12	22.23	88.35
400	13.98	20.91	83.11
500	14.65	19.56	77.74
600	15.16	18.13	72.06

Another explanation answerable for a decline in sorption percentage values at low pH is a competition between protons and the studied cations for the available sorption sites [43]. With the rise of pH of the solution, negative charged (OH^-) ions increased, and positively charged ions decreased at the surface of SiV, which brings about an attractive force between the metal ions and the surface of the SiV. Hence, the sorption percentage of the SiV was discovered to be increased at higher pH [44]. Therefore, a pH of 5.50 was chosen to conduct further sorption experiments. The obtained results demonstrated that the sorption of Eu(III) and Tb(III) ions by SiV was pH-dependent.

3.2.2. *Effect of contact time*

For examining the impact of contact time on the sorption of Eu(III) and Tb(III) ions by SiV, time was varied between 5–1,440 min keeping the rest of the parameters constant (pH 5.50, stirring speed 200 rpm, temperature 25°C ± 1°C, initial metal concentration 50 mg/L, volume 3 mL, diameter of particles, dp 0.370 mm, and sorbent weight 0.03 g).

Fig. 8 shows plots of the amount of sorbed ions from aqueous solution onto SiV as a function of contact time. The figure shows vividly that the sorption of selected metal ions has increased up to 200 min of contact time after that saturation appears and adsorption–desorption rate became equal. It was observed that in the first 60 min, the sorption rate was higher for the selected metal ions, then slow down and reached equilibrium. The initial higher rate of metal ions sorption ascribed to the unoccupied sorption sites as well as the concentration differences of the metal ions at the SiV surface and in the bulk of the solution was large. Whereas, after 60 min of contact time, the sorption rate decreased significantly due to the slowing down of the diffusion rate of cations into the interior channels of the SiV. The diffusion rate was guided by the surface coverage of the metal ions, once the SiV surface was saturated with the metal ions, the diffusion rate decreased. It can be seen from Fig. 8, after 200 min of contact time, there was a negligible or slight change in the sorption of metal ions. Therefore, 200 min was established as equilibrium time for Eu(III) and Tb(III) ions sorption onto SiV, for further experiments in this study this equilibrium time was used. The uptake of studied ions by SiV might be because of the

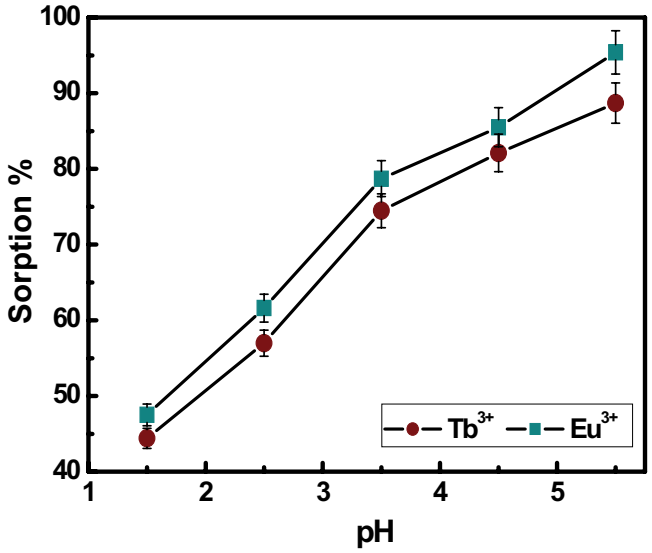

Fig. 7. Effect of pH on the sorption of Eu(III) and Tb(III) ions, at stirring speed, 200 rpm; contact time, 200 min; temperature, 25°C ± 1°C; dp = 0.370 mm; C_0, 50 mg/L; volume, 3 mL; weight, 0.03 g.

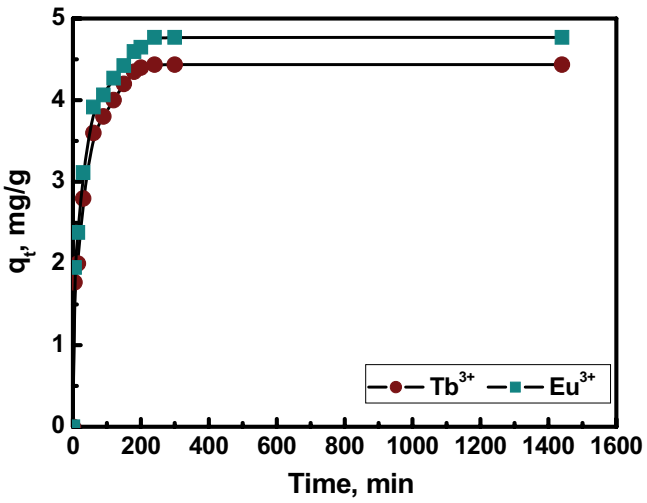

Fig. 8. Effect of contact time on the sorption of Eu(III) and Tb(III) ions, at stirring speed, 200 rpm; temperature, 25°C ± 1°C; dp = 0.370 mm; C_0, 50 mg/L; volume, 3 mL; weight, 0.03 g; pH 5.50.

sorption of the ions in the surface of SiV and/ or exchange of these ions with some H^+ on the surface of the SiV.

3.2.3. Effect of SiV weight

The impact of SiV weight on the sorption of Eu(III) and Tb(III) ions was investigated by varying sorbent weight from 0.0075 to 0.12 g/3 mL (2.5–40 g/L) and keeping other parameters constant (contact time 200 min, stirring speed 200 rpm, temperature 25°C ± 1°C, initial metal concentration 50 mg/L, volume 3 mL, diameter of particles, dp 0.370 mm, sorbent weight 0.03 g, and pH 5.50). The sorption percentage of metal ions was observed to be enhanced with an increase in sorbent weight; it was due to an increase in the number of sorption sites with the rise of sorbent weight and hence more removal occurs [30,45]. Fig. 9 shows that there is no sensible change in sorption efficiency by increasing sorbent weight more than 0.03 g related to surface saturation. Thus, 0.03 g/3 mL (i.e., 10 g/L of Eu(III) and Tb(III) ions solutions) were chosen as the best dose for the treatment process.

3.2.4. Effect of initial metal concentration

The metal ion concentrations were varied from 50 to 500 mg/L, and their effect was observed on a fixed dosage of the sorbent (10 g/L) as appears in Fig. 10. As per this figure, increasing the Eu(III) and Tb(III) initial concentration reduced the sorption yield. Under the optimized condition, the highest sorption efficiency was acquired utilizing the initial concentration of 50 mg/L. It very well may be clarified as far as available sorption sites are limited in the solution for higher metal ions concentrations [30]. This study revealed that the best-achieved sorption yield was 95.40% and 88.70% for Eu(III) and Tb(III) ions, respectively using an initial concentration of 50 mg/L of Eu(III) and Tb(III) ions.

3.3. Sorption isotherms

The sorption isotherm experiments were accomplished by shaking 3 mL from metal ion solutions of different concentrations (50–500 mg/L) with 0.03 g of SiV for 200 min, at pH 5.50. Non-linear Langmuir, Freundlich, Dubinin–Radushkevich, and Temkin isotherm models were utilized to depict the isothermal properties of the sorbent. However, the Langmuir isotherm considers adsorption as a chemical phenomenon, assuming that all the available adsorption active sites are similar, the adsorbed species do not interact, and a monolayer is formed during adsorption [46]. Freundlich, on the other hand, valid for physical adsorption and applies to adsorption on heterogeneous surfaces with the interaction between the adsorbed molecules, and is not restricted to the formation of a monolayer [47–49]. The Dubinin–Radushkevich isotherm model is more general than the Langmuir isotherm because it does not assume a homogeneous surface or constant sorption potential [50]. This model was used to estimate the mean free energy of sorption (E_{DR}), which was used to find out the sorption mechanism whether it is physical or chemical adsorption or ion exchange. The Temkin isotherm model predicts a uniform distribution of binding energies over the population of surface binding adsorption, it applies to chemical adsorption only [51]. Also, it was chosen to determine the adsorption potentials of the adsorbent for adsorbates [52].

$$\left(E_{DR} = \frac{1}{\sqrt{2\beta_{DR}}} \right)$$

The non-linear form of Langmuir, Freundlich, Dubinin–Radushkevich, and Temkin sorption isotherms can be expressed by Eqs. (6)–(9), respectively;

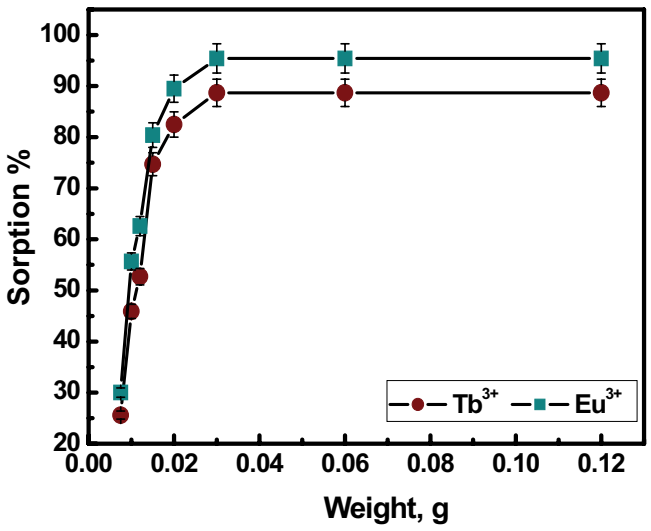

Fig. 9. Effect of SiV weight on the sorption of Eu(III) and Tb(III) ions, at stirring speed, 200 rpm; contact time, 200 min; temperature, 25°C ± 1°C; dp = 0.370 mm; C_0, 50 mg/L; volume, 3 mL; pH 5.50.

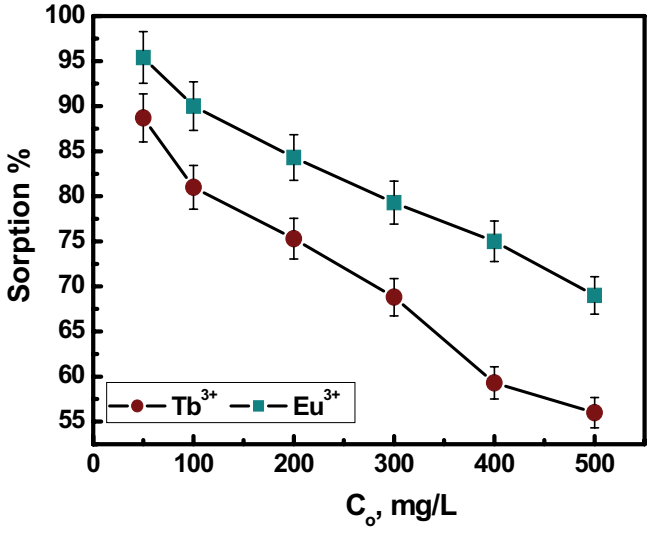

Fig. 10. Effect of initial metal concentrations on the sorption of Eu(III) and Tb(III) ions, at stirring speed, 200 rpm; contact time, 200 min; temperature, 25°C ± 1°C; dp = 0.370 mm; volume, 3 mL; weight, 0.03 g; pH 5.50.

$$q_e = \frac{q_m k_L C_e}{1 + K_L C_e} \quad (6)$$

$$q_e = k_f C_e^{1/n} \quad (7)$$

$$q_e = q_{DR} \exp\left(-\beta_{DR} \varepsilon^2\right) \quad (8)$$

$$q_e = \frac{RT}{b_t} \ln\left(a_t C_e\right) \quad (9)$$

In these equations, q_e (mg/g) and C_e (mg/L) is the adsorbed amount by the adsorbent and concentration of Eu(III) and Tb(III) in solution at equilibrium conditions, respectively. The K_L (L/mg) and q_m (mg/g) are constants related to the affinity of adsorptive sites and the maximum adsorption capacity of the adsorbent, respectively. The k_f (mg/g) and n are Freundlich constants associated with adsorption capacity and intensity, respectively. The β_{DR} (mol²/kJ²) is Dubinin–Radushkevich constant, q_{DR} (mg/g) is the theoretical adsorption capacity, ε is the Polanyi potential = $RT\ln(1 + 1/C_e)$, T is the absolute temperature (K), and R is the universal gas constant, 8.314 J/mol K. The a_t (L/g) is Temkin isotherm equilibrium binding constant and b_t (J/mol) is constant corresponding to the heat of sorption = RT/b_t.

The non-linear plots of these isotherm models are shown in Fig. 11 and the obtained model parameters are summarized in Table 5. The correlation coefficient, R^2 determined from the Freundlich and Langmuir models ($R^2 > 98$) were higher than that determined from the Temkin and Dubinin–Radushkevich models. Furthermore, the chi-square (χ^2) values of the Freundlich and Langmuir isotherm models are smaller than those of the other models, implying that the calculated k_f (Freundlich capacity) and q_m (Langmuir monolayer capacity) are more compatible with the experimental adsorption capacity [45]. The correlation coefficient, R^2 determined from the Dubinin–Radushkevich model is low ($R^2 < 81$) confirming that the non-applicability of this model.

Based on these results, it can be concluded that the Freundlich and Langmuir isotherm models are more proper for the illumination of the relationship between q_e and C_e compared to the Temkin, and Dubinin–Radushkevich models. The maximum monolayer capacity, q_m obtained from non-linear Langmuir plots for Eu(III) and Tb(III) ions was discovered to be 44.23 and 34.39 mg/g respectively. These values are very reasonable compared to their counterparts obtained from other sorbents as appeared in Table 6. In this manner, it very well may be concluded that the SiV sorbent material has important potential for retention of Eu(III) and Tb(III) ions from waste solutions.

3.4. Sorption kinetics

Kinetic investigations were carried out using the solutions with the volume of 3 mL prepared at 50 mg/L of Eu(III) and Tb(III) ions that were contacted with 0.03 g of the sorbent at various times. The experiments were conducted in a mono element system. Therefore, knowing of the sorption reaction mechanism and diffusion mechanism is essential. In this respect, three different kinetic models namely, pseudo-first-order, pseudo-second-order, and intra-particle diffusion were applied to the experimental data. These models are employed to fit the experimental data for the prediction of the kinetic parameters as following [65–68]:

Pseudo-first-order:

$$\ln\left(q_e - q_t\right) = \ln q_e - k_1 t \quad (10)$$

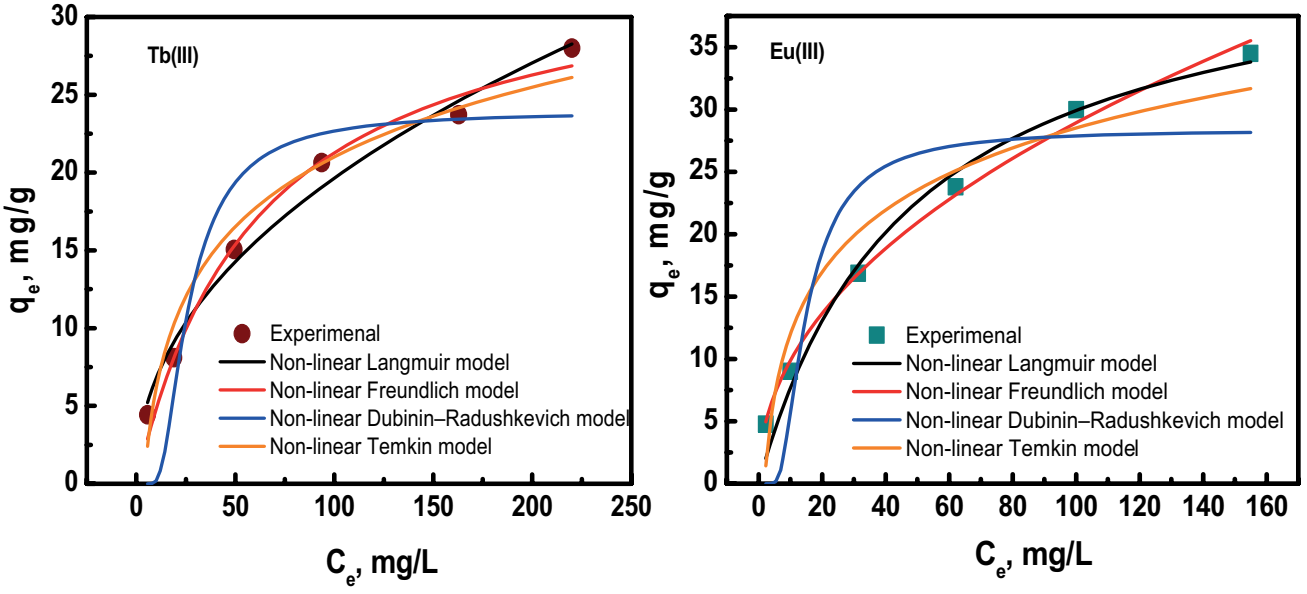

Fig. 11. Non-linear Langmuir, Freundlich, Dubinin–Radushkevich, and Temkin isotherm models for sorption of Eu(III) and Tb(III) onto SiV.

Table 5
Isotherm parameters of different models for Eu(III) and Tb(III) sorption onto SiV exchanger at 25°C ± 1°C

Isotherm models	Non-linear regression	Parameters	Eu(III))	Tb(III)
Langmuir isotherm	$q_e = \frac{q_m k_L C_e}{1 + K_L C_e}$	q_m (mg/g)	44.23	34.39
		K_L (L/mg)	0.021	0.016
		R^2	0.98570	0.98435
		χ^2	1.58	1.31
Freundlich isotherm	$q_e = k_f C_e^{1/n}$	k_f (mg/g)	3.36	2.34
		$1/n$	0.467	0.461
		R^2	0.99392	0.98278
		χ^2	0.84	1.45
Dubinin–Radushkevich isotherm	$q_e = q_{DR} \exp\left(-\beta_{DR}\varepsilon^2\right)$	q_{DR} (mg/g)	28.38	23.91
		β_{DR} (mol²/kJ²)	0.02906	0.08758
		E_{DR} (kJ/mol)	4.15	2.39
		R^2	0.74862	0.80606
		χ^2	34.55	16.27
Temkin isotherm	$q_e = \frac{RT}{b_t}\ln\left(a_t C_e\right)$	a_t (L/g)	0.53	0.26
		b_t	344.88	382.77
		b_t (J/mol)	7.18	6.47
		R^2	0.92151	0.95698
		χ^2	10.79	3.61

Table 6
Comparison of Eu(III) and Tb(III) adsorption capacity for various sorbents

Adsorbents	Maximum adsorption capacity, mg/g		References
	Eu(III)	Tb(III)	
Hydroxyl magnesium silicate	4.00	NR	[53]
D155 resin	357.00	NR	[54]
Magnetic alginate/hydroxyapatite biopolymeric composite	250.00	NR	[55]
$BaCO_3$	16.00	NR	[56]
Activated carbon	18.41	NR	[57]
CA/PEG	27.40	NR	[58]
RF resin	72.9	NR	[17]
HCR resin	76.40	NR	[59]
TVEX-PHOR resin	NR	30.49	[60]
CMC/P(PTA)/$Ni_{0.2}Zn_{0.2}Fe_{2.6}O_4$	NR	42.87	[61]
CA/CMC/$Ni_{0.2}Zn_{0.2}Fe_{2.6}O_4$	NR	88.61	[62]
CA/CMC/$Ni_{0.2}Zn_{0.2}Fe_{2.6}O_4$	NR	24.41	[63]
CA-P(P-T-A)-NZFO	NR	98.34	[64]
SiV	44.23[a]	34.39[a]	Current work

NR: not reported;
[a]Calculated from Langmuir isotherm.

Pseudo-second-order:

$$\frac{t}{q_t} = \frac{1}{k_2 q_e^2} + \frac{t}{q_e} \tag{11}$$

Intraparticle diffusion:

$$q_t = k_{id} t^{0.5} + C \tag{12}$$

where q_e (mg/g) and q_t (mg/g) are defined as the amount of adsorbate per gram of the adsorbent at equilibrium and t time, respectively. k_1 (min^{-1}), k_2 (g/mg min), and k_{id} (mg/g min$^{1/2}$) respectively refer to the pseudo-first-order, pseudo-second-order, and intraparticle diffusion rate constants. Moreover, C provides information about the thickness of the boundary layer, since the resistance to the external mass transfer increases as the intercept increases [69].

The values of kinetic parameters obtained from Fig. 12 are shown in Table 7. As it is obvious from the results, the highest values of R^2 and the remarkable agreement between the theoretical and experimental q_e obtained by pseudo-second-order shows that the main mechanism for controlling the sorption of Eu(III) and Tb(III) ions onto the prepared SiV is chemisorption [63]. According to the intraparticle diffusion model, the plot of q_t, vs. $t^{0.5}$ should be linear if intraparticle diffusion is involved in the sorption process and will pass through the origin if intraparticle diffusion is the rate-controlling step. In the current case, the linear plots not passing through origin were obtained suggesting the involvement of intraparticle diffusion in the sorption process but not as the sole rate-limiting step. The sorption process is complex and external mass transfer may also be involved in the procedure [70,71].

3.5. Thermodynamic evaluation

In order to expose the dependency of Eu(III) and Tb(III) sorption on temperature, some thermodynamic parameters such as enthalpy change ($\Delta H°$), entropy change ($\Delta S°$), and free energy change ($\Delta G°$) were calculated from the experimental data at 298, 318, and 338 K. The $\Delta G°$ parameter was calculated based on the adsorption distribution constant K_d (q_e/C_e) as shown below [29]:

$$\Delta G° = -RT \ln K_d \tag{13}$$

The values of $\Delta H°$ and $\Delta S°$ were determined from the slope and intercept of the straight line obtained from plotting $\ln K_d$ vs. $1/T$, respectively for all of the studied temperatures (Fig. 13).

$$\ln K_d = \left(\frac{\Delta S°}{R}\right) - \left(\frac{\Delta H°}{RT}\right) \tag{14}$$

The value of $\Delta G°$ was calculated as –1.81, –3.94, and –6.43 kJ/mol for Eu(III) and 0.60, –0.19, and –1.26 kJ/mol for Tb(III) at 298, 318, and 338 K, respectively. The acquired negative values of $\Delta G°$ affirm the feasibility of the process and the spontaneous nature of the sorption processes.

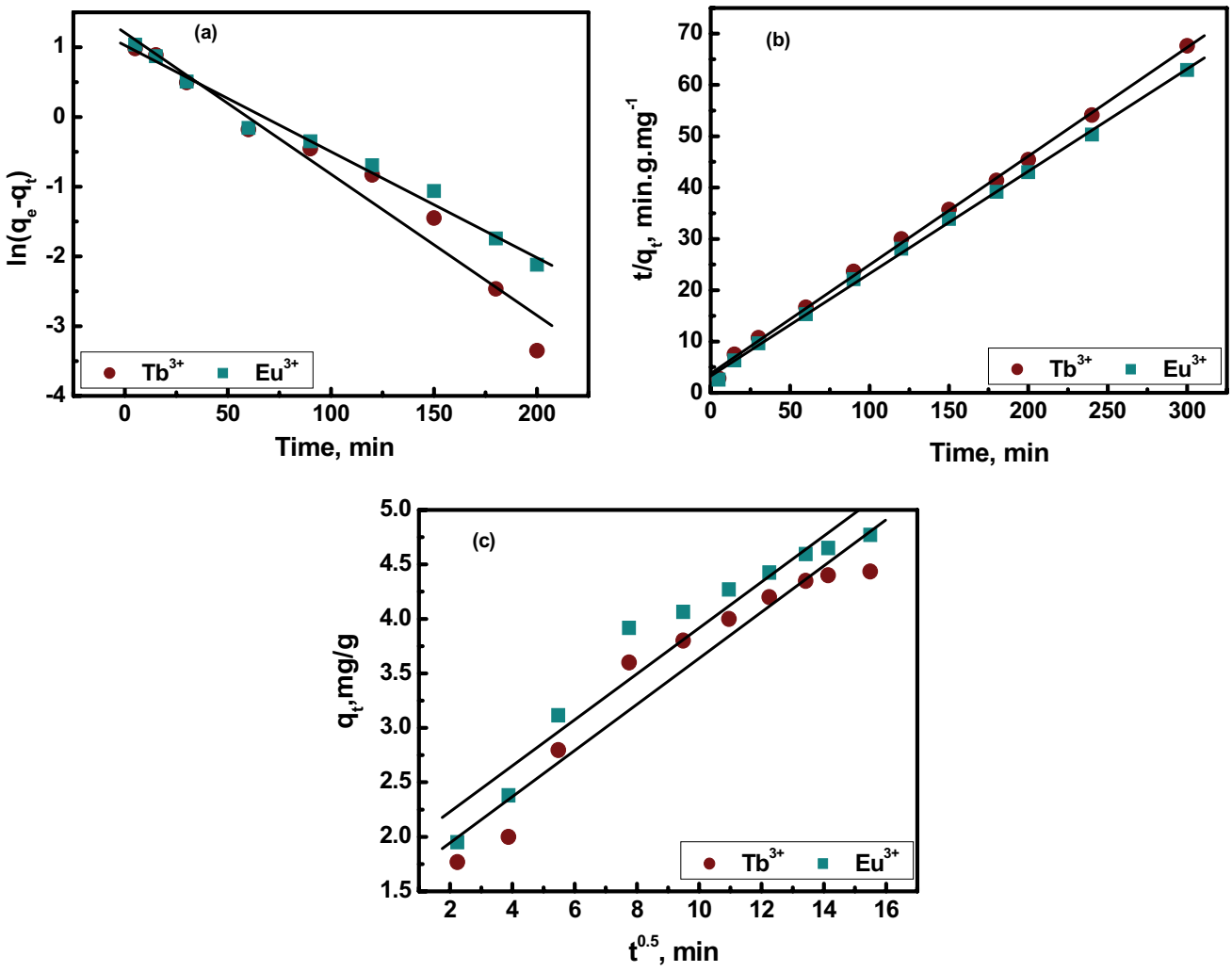

Fig. 12. Kinetic plots obtained from (a) pseudo-first-order model, (b) pseudo-second-order model, and (c) intraparticle diffusion at 25°C ± 1°C.

Table 7
Kinetic parameters obtained from pseudo-first-order, pseudo-second-order, and intraparticle diffusion models for sorption of Eu(III) and Tb(III) onto SiV exchanger at 25°C ± 1°C

Cation	$q_{e,exp}$ (mg/g)	Pseudo-first-order kinetic model			Pseudo-second-order kinetic model			Intraparticle diffusion		
		k_1 (min^{-1})	q_e (mg/g)	R^2	k_2 (g/mg min)	q_e (mg/g)	R^2	k_{id} (mg/g $min^{1/2}$)	C	R^2
Eu(III)	4.77	0.0152	2.78	0.99231	0.0121	5.01	0.99921	0.2109	1.809	0.96444
Tb(III)	4.40	0.0203	3.34	0.98185	0.0119	4.72	0.99915	0.2118	1.521	0.96447

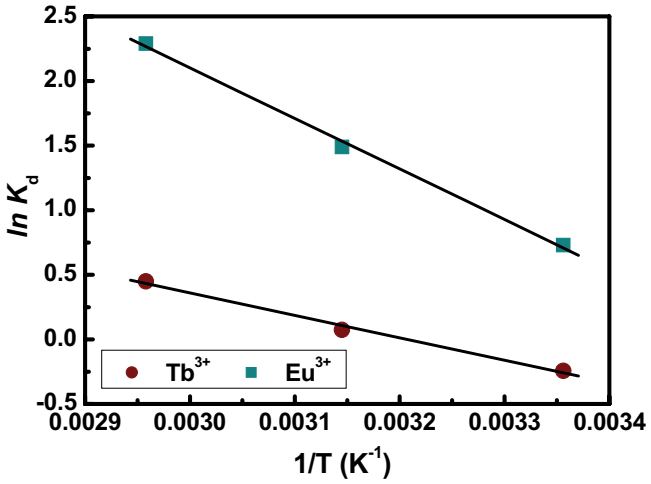

Fig. 13. Plot of $\ln K_d$ vs. $1/T$ for the estimation of thermodynamic parameters.

The increase in negative values of $\Delta G°$ with increasing the temperature (Table 8) means that the spontaneity and feasibility of Eu(III) and Tb(III) sorption were increased with boosting the temperature of the solution, this behavior is not consistent with the sorption behavior of U(VI) onto PC-g-P(TMC-M) [29] and Th(IV) onto CNF-ETA-TMC [72]. By considering the slope and intercept of the plot in Fig. 13, $\Delta H°$ and $\Delta S°$ parameters were calculated and summarized in Table 8. The change in $\Delta H°$ for Eu(III) and Tb(III) ions was discovered to be positive values confirming the endothermic nature of the sorption process. The positive values of $\Delta S°$ suggest increased randomness at the solid/solution interface with an increase in the degree of freedom of the sorbed species.

3.6. Application

One of the great dangers facing humans and different animals is a pollution of the environment with pollutants, whether radioactive or non-radioactive. Among the most important pollutants are those that are produced from nuclear applications [73,74]. The removal efficiency of the prepared SiV towards $^{152+154}$Eu and ^{160}Tb radionuclides solution were tested using batch technique under the optimum conditions, known volume (3 mL) of this solution was mixed with (0.03 g) of SiV exchanger as optimum weight at 25°C ± 1°C. The mixture was intermittently shaken at a constant agitation speed of 200 rpm for 200 min. After shaking, the SiV exchanger was separated and the supernatant was analyzed radiometrically. The decontamination factor was computed utilizing the next equation;

$$DF = \frac{A_i}{A_f} \quad (15)$$

where (A_i) and (A_f) are the initial and final activities (Bq/mL) of the radioactive solution respectively.

Data obtained are introduced in Table 9. It can be seen that the radioisotope $^{152+154}$Eu has the highest decontamination factor (5.60) compared to ^{160}Tb (3.81). The employment of SiV has shown that all radionuclides can be wonderfully separated from these samples with percent removals ranged from 73% to about 82% with just one treatment. The results offered that SiV exchanger could be counted to be an exceedingly effective and helpful material for other lanthanides or trivalent actinides such as ^{241,242m,243}Am removal from wastewaters or real radioactive waste.

3.7. Desorption studies

Desorption or elimination of the adsorbate from the adsorbent surface makes it possible to regenerate the adsorbent and recycling the adsorbate. Desorption of Eu(III) and Tb(III) ions from loaded SiV is commonly completed utilizing different mineral acids from 0.01 to 0.5 mol/L. In each experiment, 0.03 g of SiV loaded with Eu(III) or Tb(III) ions was vigorously shacked with 3 mL mineral acids of desired concentration for 200 min at 25°C ± 1°C. Utilizing the mineral acids, for example, HCl and HNO_3 make the sorbent surface rich with protons (H^+). Then, the H^+ can remove more easily the positively charged metal ions, thus leading to the desorption of adsorbed ions by ion exchange mechanism [60]. As depicted in Fig. 14, the recovery of Eu(III) and Tb(III) ions from loaded SiV increased with increasing the HNO_3 concentration till 0.4 mol/L HNO_3. Further increase in the HNO_3 concentration does not affect the desorption of Eu(III) and Tb(III) ions. 0.4 mol/L HNO_3 can be utilized as a decent desorbing reagent to elute the adsorbed metal ions from SiV ion exchange material with the highest desorption percentage of 87.11% and 80.60% for Eu(III) and Tb(III), respectively after one step desorption. When metal-SiV adsorbed was treated with nitric acid of 0.4 mol/L, a desorption process was proceeded due to a competition between hydrogen ion provided by the HNO_3 solution and the cationic form of the metal ions, which makes active sites occupied by H^+. It affects the association of the resin with metals and most of Eu(III) or Tb(III) returns to the solution. Subsequently, 0.4 mol/L HNO_3 can be considered as a promising eluent for Eu(III) and Tb(III), and the reuse of resin remains significant.

Table 8
Thermodynamic parameters for sorption of Eu(III) and Tb(III) from aqueous solution onto SiV exchanger at different reaction temperatures

Cation	Temp. (K)	ΔG° (kJ/mol)	ΔH° (kJ/mol)	ΔS° (J/mol K)
Eu(III)	298	–1.81	32.53	115.06
	318	–3.94		
	338	–6.43		
Tb(III)	298	0.60	14.43	46.28
	318	–0.19		
	338	–1.26		

Table 9
Radiometric measurements for Eu-152+154 and Tb-160 sorbed onto SiV exchanger to determine the sorption percent and decontamination factor

Ion	A_0	A_f	Sorption %	D.F.
Eu-152+154	3,657	653	82.14	5.60
Tb-160	2,445	642	73.74	3.81

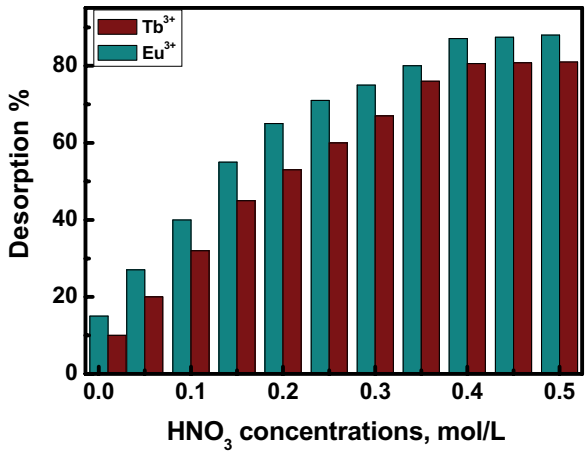

Fig. 14. Recovery of Eu(III) and Tb(III) from loaded SiV exchanger using different concentrations from HNO_3.

4. Conclusions

In view of the results mentioned above, the following conclusions can be pointed out:

- Silico vanadate was prepared as a new and novel crystalline inorganic ion exchanger which possesses high chemical and thermal stabilities.
- XRD patterns and TEM photographs confirm that more than one component agglomerate with each other; a large vanadate component is intimately mixed with nano-sized silica.
- FT-IR and pH titration studies indicate that Si–O–H and V–O–H groups are responsible for releasing its H^+ ions to be exchanged with the studied cations.
- The SiV ion exchange material is a potential material for the removal of Eu(III) and Tb(III) from aqueous solution with sorption of 95.40% and 88.70%, respectively within 200 min.
- Both Freundlich and Langmuir models were the best fit models to depict the sorption equilibrium and the maximum monolayer capacity (q_m) was 44.23 and 34.39 mg/g for Eu(III) and Tb(III), respectively at 25°C ± 1°C using non-linear Langmuir plots.
- The experimental data are in good conformity with the pseudo-second-order and the intraparticle diffusion mass transfer kinetic models.
- The sorption of Eu(III) and Tb(III) by SiV was spontaneous and endothermic in nature.
- Desorption studies indicated that both metal ions can be disposed of from the used sorbent using 0.4 mol/L HNO_3 solution and SiV can be regenerated and reused for further sorption processes.

References

[1] P. Maestro, D. Huguenin, Industrial applications of rare earths: which way for the end of the century, J. Alloys Compd., 225 (1995) 520–528.
[2] M.M. Hamed, M.A. Hilal, E.H. Borai, Chemical distribution of hazardous natural radionuclides during monazite mineral processing, J. Environ. Radioact., 162–163 (2016) 166–171.
[3] E.S.C. Emmanuel, T. Ananthi, B. Anandkumar, S. Maruthamuthu, Accumulation of rare earth elements by siderophore-forming *Arthrobacter luteolus* isolated from rare earth environment of Chavara, India, J. Biosci., 37 (2012) 25–31.
[4] R. Akkaya, Synthesis and characterization of a new low-cost composite for the adsorption of rare earth ions from aqueous solutions, Chem. Eng. J., 200–202 (2012) 186–191.
[5] C. Müller, E. Fischer, M. Behe, U. Köster, H. Dorrer, J. Reber, S. Haller, S. Cohrs, A. Blanc, J. Grünberg, M. Bunka, K. Zhernosekov, N. van der Meulen, K. Johnston, A. Türler, R. Schibli, Future prospects for SPECT imaging using the radiolanthanide terbium-155 - production and preclinical evaluation in tumor-bearing mice, Nucl. Med. Biol., 41 (2013) e58–e65.
[6] C. Müller, C. Vermeulen, K. Johnston, U. Köster, R. Schmid, A. Türler, N.P. van der Meulen, Preclinical in vivo application of ^{152}Tb-DOTANOC: a radiolanthanide for PET imaging, EJNMMI Res., 6 (2016) 1–10, doi: 10.1186/s13550-016-0189-4.
[7] C. Müller, J. Reber, S. Haller, H. Dorrer, P. Bernhardt, K. Zhernosekov, A. Türler, R. Schibli, Direct in vitro and in vivo comparison of ^{161}Tb and ^{177}Lu using a tumour-targeting folate conjugate, Eur. J. Nucl. Med. Mol. Imaging, 41 (2014) 476–485.
[8] C. Müller, K. Zhernosekov, U. Köster, K. Johnston, H. Dorrer, A. Hohn, N.T. van der Walt, A. Türler, R. Schibli, A unique matched quadruplet of terbium radioisotopes for PET and SPECT and for α- and β- radionuclide therapy: an in vivo

proof-of-concept study with a new receptor-targeted folate derivative, J. Nucl. Med., 53 (2012) 1951–1959.
[9] G.F. Steyn, C. Vermeulen, F. Szelecsényi, Z. Kovács, A. Hohn, N.P. van der Meulen, R. Schibli, T.N. van der Walt, Cross sections of proton-induced reactions on ^{152}Gd, ^{155}Gd and ^{159}Tb with emphasis on the production of selected Tb radionuclides, Nucl. Instrum. Methods Phys. Res., Sect. B, 319 (2014) 128–140.
[10] Z. Kovács, F. Szelecsényi, K. Brezovcsik, Preparation of thin gadolinium samples via electrodeposition for excitation function studies, J. Radioanal. Nucl. Chem., 307 (2016) 1861–1864.
[11] S. Lehenberger, C. Barkhausen, S. Cohrs, E. Fischer, J. Grünberg, A. Hohn, U. Köster, R. Schibli, A. Türler, K. Zhernosekov, The low-energy β^- and electron emitter ^{161}Tb as an alternative to ^{177}Lu for targeted radionuclide therapy, Nucl. Med. Biol., 38 (2011) 917–924.
[12] A. Ahlem, M. Samira, E.H. Ali, G. Pierre, T. Leila, Intracellular behavior of samarium and europium in lactating mammary gland, J. Rare Earths, 30 (2012) 274–277.
[13] L.C. Courrol, M.H. Bellini, L.V.G. Tarelho, F.R.O. Silva, R.D. Mansano, L. Gomes, N.D. Veira Jr., N. Shor, Urea hydrogen peroxide determination in whole blood using europium tetracycline probe, Anal. Biochem., 355 (2006) 140–144.
[14] S. Ghose, E. Trinquet, M. Laget, H. Bazin, G. Mathis, Rare earth cryptates for the investigation of molecular interactions *in vitro* and in living cells, J. Alloys Compd., 451 (2008) 35–37.
[15] A. Rout, K.A. Venkatesan, T.G. Srinivasan, P.R. Vasudeva Rao, Extraction behavior of actinides and fission products in amide functionalized ionic liquid, Sep. Purif. Technol., 97 (2012) 164–171.
[16] K. Roy, P. Sinha, S. Lahiri, Immobilization of long-lived radionuclides ^{152,154}Eu by selective bioaccumulation in *Saccharomyces cerevisiae* from a synthetic mixture of ^{152,154}Eu, ^{137}Cs and ^{60}Co, Biochem. Eng. J., 40 (2008) 363–367.
[17] M.F. Attallah, E.H. Borai, S.A. Shady, Kinetic investigation for sorption of europium and samarium from aqueous solution using resorcinol–formaldehyde polymeric resin, J. Radioanal. Nucl. Chem., 299 (2014) 1927–1933.
[18] J.S. Kim, C.H. Lee, S.H. Han, M.Y. Suh, Studies on complexation and solvent extraction of lanthanides in the presence of diaza-18-crown-6-di-isopropionic acid, Talanta, 45 (1997) 437–444.
[19] J.G. Sen Gupta, Determination of scandium, yttrium and lanthanides in silicate rocks and four new canadian iron-formation reference materials by flame atomic-absorption spectrometry with micro sample injection, Talanta, 31 (1984) 1045–1051.
[20] C.H. Xiong, X.Z. Liu, C.P. Yao, Effect of pH on sorption for RE(III) and sorption behaviors of Sm(III) by D152 resin, J. Rare Earths, 26 (2008) 851–856.
[21] M.M. Hamed, S.E. Rizk, A.A. Nayl, Adsorption kinetics and modeling of gadolinium and cobalt ions sorption by an ion-exchange resin, Part. Sci. Technol., 34 (2016) 716–724.
[22] C.P. Yao, Adsorption and desorption properties of D151 resin for Ce(III), J. Rare Earths, 28 (2010) 183–188.
[23] C.H. Xiong, Z.W. Zheng, Evaluation of D113 cation exchange resin for the removal of Eu(III) from aqueous solution, J. Rare Earths, 28 (2010) 862–867.
[24] M. Qureshsiy, S.A. Nabia, N. Zehra, Synthesis, ion-exchange properties, and analytical applications of thermally stable tin(IV) vanadate, Can. J. Chem., 55 (1977) 1667–1672.
[25] N.E. Topp, K.W. Pepper, Properties of ion-exchange resins in relation to their structure. Part I. Titration curves, J. Chem. Soc., 690 (1949) 3299–3303.
[26] E.A. Abdel-Galil, A.S. Tourky, A.E. Kasem, Sorption of some radionuclides from nuclear waste effluents by polyaniline/SiO_2 composite: characterization, thermal stability, and gamma irradiation studies, Appl. Radiat. Isot., 156 (2020) 109009, doi: 10.1016/j.apradiso.2019.109009.
[27] R. Neumann, M. Levin-Elad, Vanadium silicate xerogels in hydrogen peroxide catalyzed oxidations, Appl. Catal., A, 122 (1995) 85–97.
[28] F. Mani, J.A. Sawada, S.M. Kuznicki, Spontaneous formation of silver nanoparticles on the vanadium silicate EVS-10, Microporous Mesoporous Mater., 224 (2016) 208–216.
[29] M. Tuzen, T.A. Saleh, A. Sarı, Naeemullah, Interfacial polymerization of trimesoyl chloride with melamine and palygorskite for efficient uranium ions ultra-removal, Chem. Eng. Res. Des., 159 (2020) 353–361.
[30] M.M. Hamed, A.M. Shahr El-Din, E.A. Abdel-Galil, Nanocomposite of polyaniline functionalized Tafla: synthesis, characterization, and application as a novel sorbent for selective removal of Fe(III), J. Radioanal. Nucl. Chem., 322 (2019) 663–676.
[31] P.R. Hari Prasad Rao, A.V. Ramaswamy, P. Ratnasamy, Synthesis and catalytic properties of crystalline, microporous vanadium silicates with MEL Structure, J. Catal., 137 (1992) 225–231.
[32] Taylor, X-ray Metallography, John Wiley, New York, 1961, pp. 678–686.
[33] D. Gruber, F. Kraus, J. Müller, A novel gas sensor design based on $CH_4/H_2/H_2O$ plasma etched ZnO thin films, Sens. Actuators, B, 92 (2003) 81–89.
[34] T.A. Saleh, Naeemullah, M. Tuzen, A. Sarı, Polyethylenimine modified activated carbon as novel magnetic adsorbent for the removal of uranium from aqueous solution, Chem. Eng. Res. Des., 117 (2017) 218–227.
[35] M.M. Abd El-Latif, M.F. El-Kady, Developing & characterization of a new zirconium vanadate ion exchanger and its novel organic-inorganic hybrid, J. Appl. Sci. Res., 4 (2008) 1–13.
[36] F. Mani, L. Wu, S.M. Kuznicki, A simplified method to synthesize pure vanadium silicate analogue of ETS-10, Microporous Mesoporous Mater., 177 (2013) 91–96.
[37] E.A. Abdel-Galil, M.A. Eid, R.S. Hassan, Preparation of nanosized stannic silicomolybdate for chromatographic separation of Y(III) from Zr(IV), Part. Sci. Technol., 38 (2020) 113–120.
[38] S.A. Nabi, A.M. Khan, Synthesis, ion exchange properties and analytical applications of stannic silicomolybdate: effect of temperature on distribution coefficients of metal ions, React. Funct. Polym., 66 (2006) 495–508.
[39] I.M. El-Naggar, E.A. Mowafy, E.A. Abdel-Galil, M.F. El-Shahat, Synthesis, characterization and ion-exchange properties of a novel 'organic–inorganic' hybrid cation-exchanger: polyacrylamide Sn(IV) molybdophosphate, Global J. Phys. Chem., 1 (2010) 91–106.
[40] I.M. El-Naggar, K.A. Hebash, E.S. Sheneshen, E.A. Abdel-Galil, Preparation, characterization and ion-exchange properties of a new 'organic–inorganic' composite cation exchanger polyaniline silicotitanate: its applications for treatment of hazardous metal ions from waste solutions, Inorg. Chem. Indian J., 9 (2014) 1–14.
[41] A.S. Tourky, E.A. Abdel-Galil, A.E. Kasem, N. Belacy, Synthesis and application of polyacrylamide Sn(IV) silicovanadate for sorption of some radionuclides, J. Nucl. Technol. Appl. Sci., 4 (2016) 35–50.
[42] E.A. Abdel-Galil, G.E. Sharaf El-Deen, Y.F. El-Aryan, M. Khalil, Preparation of hybrid ion exchanger based on acrylamide for sorption of some toxic metal ions from aqueous waste solutions, Russ. J. Appl. Chem., 89 (2016) 467–479.
[43] S.Z. Mohammadi, M.A. Karimi, D. Afzali, F. Mansouri, Removal of Pb(II) from aqueous solutions using activated carbon from Sea-buckthorn stones by chemical activation, Desalination, 262 (2010) 86–93.
[44] E.A. Abdel-Galil, W.M. El-Kenany, L.M.S. Hussin, Preparation of nanostructured hydrated antimony oxide using a sol-gel process. Characterization and applications for sorption of La^{3+} and Sm^{3+} from aqueous solutions, Russ. J. Appl. Chem., 88 (2015) 1351–1360.
[45] E.A. Abdel-Galil, R.S. Hassan, M.A. Eid, Assessment of nano-sized stannic silicomolybdate for the removal of ^{137}Cs, ^{90}Sr, and ^{141}Ce radionuclides from radioactive waste solutions, Appl. Radiat. Isot., 148 (2019) 91–101.
[46] I. Langmuir, The adsorption of gases on plane surfaces of glass, mica and platinum, J. Am. Chem. Soc., 40 (1918) 1361–1403.
[47] H.M.F. Freundlich, Over the adsorption in solution, J. Phys. Chem., 57 (1906) 385–470.

[48] M.M. Hamed, S.M. Yakout, H.S. Hassan, Solid phase extraction of nitrate and nitrite anions using naturally and available sorbent, J. Radioanal. Nucl. Chem., 295 (2013) 697–708.
[49] M.F. Attallah, H.S. Hassan, M.A. Youssef, Synthesis and sorption potential study of Al_2O_3-ZrO_2-CeO_2 composite material for removal of some radionuclides from radioactive waste effluent, Appl. Radiat. Isot., 147 (2019) 40–47.
[50] A.E.M. Hussein, A.M.A. Morsy, Uranium recovery from wet-process phosphoric acid by a commercial ceramic product, Arabian J. Chem., 10 (2017) S361–S367.
[51] L.C. Lau, N.M. Nor, K.T. Lee, A.R. Mohamed, Adsorption isotherm, kinetic, thermodynamic and breakthrough curve models of H_2S removal using CeO_2/NaOH/PSAC, Int. J. Petrochem. Sci. Eng., 1 (2016) 00009.
[52] C. Theivarasu, S. Mylsamy, Removal of malachite green from aqueous solution by activated carbon developed from cocoa (*Theobroma Cacao*) shell – a kinetic and equilibrium studies, E-J. Chem., 8 (2011) S363–S371.
[53] M.M. Hamed, M. Holiel, I.M. Ahmed, Sorption behavior of cesium, cobalt and europium radionuclides onto hydroxyl magnesium silicate, Radiochim. Acta, 104 (2016) 873–890.
[54] X. Chunhua, M. Yuan, Y. Caiping, Characters of kinetic and equilibrium of adsorption of Eu(III) by an cation exchange resin, Iran. J. Chem. Chem. Eng., 30 (2011) 97–105.
[55] C. GÖK, Equilibrium, kinetic and thermodynamic studies of europium adsorption by biopolymeric composite, Int. J. Chem. Eng. Appl., 8 (2017) 334–339.
[56] F. Granados-Correa, M. Jiménez-Reyes, Combustion synthesis of $BaCO_3$ and its application for Eu(III) adsorption from aqueous solution, Sep. Sci. Technol., 46 (2011) 2360–2366.
[57] H.A. Omar, H. Moloukhia, Use of activated carbon in removal of some radioisotopes from their waste solutions, J. Hazard. Mater., 157 (2008) 242–246.
[58] A.A. Zaki, T. El-Zakla, M. Abed El Geleel, Modeling kinetics and thermodynamics of Cs^+ and Eu^{3+} removal from waste solutions using modified cellulose acetate membranes, J. Membr. Sci., 401–402 (2012) 1–12.
[59] M.M. Hamed, M. Holiel, Z.H. Ismail, Removal of ^{134}Cs and $^{152+154}Eu$ from liquid radioactive waste using Dowex HCR-S/S, Radiochim. Acta, 104 (2016) 399–413.
[60] H.A. Madbouly, N.E. El-Hefny, Y.A. El-Nadi, Adsorption and separation of terbium(III) and gadolinium(III) from aqueous nitrate medium using solid extractant, Sep. Sci. Technol., 56 (2021) 681–693.
[61] H. Javadian, M. Ruiz, M. Taghavi, A.M. Sastre, Synthesis of magnetic CMC bionanocomposite containing a novel biodegradable nanoporous polyamide selectively synthesized in ionic liquid as green media: investigation on Nd^{+3}, Tb^{+3}, and Dy^{+3} rare earths adsorption, J. Mol. Liq., 308 (2020) 113017, doi: 10.1016/j.molliq.2020.113017.
[62] H. Javadian, M. Ruiz, T.A. Saleh, A.M. Sastre, Ca-alginate/carboxymethyl chitosan/$Ni_{0.2}Zn_{0.2}Fe_{2.6}O_4$ magnetic bionanocomposite: synthesis, characterization and application for single adsorption of Nd^{+3}, Tb^{+3}, and Dy^{+3} rare earth elements from aqueous media, J. Mol. Liq., 306 (2020) 112760, doi: 10.1016/j.molliq.2020.112760.
[63] H. Javadian, M. Ruiz, A.M. Sastre, Response surface methodology based on central composite design for simultaneous adsorption of rare earth elements using nanoporous calcium alginate/carboxymethyl chitosan microbiocomposite powder containing $Ni_{0.2}Zn_{0.2}Fe_{2.6}O_4$ magnetic nanoparticles: batch and column studies, Int. J. Biol. Macromol., 154 (2020) 937–953.
[64] H. Javadian, M. Ruiz, M. Taghavi, A.M. Sastre, Novel magnetic nanocomposite of calcium alginate carrying poly(pyrimidine-thiophene-amide) as a novel green synthesized polyamide for adsorption study of neodymium, terbium, and dysprosium rare-earth ions, Colloids Surf., A, 603 (2020) 125252, doi: 10.1016/j.colsurfa.2020.125252.
[65] S. Lagergren, Zurtheorie der sogenannten adsorption geloster stoffe, Kungl. Svens. Vetenskapsakad. Handl., 24 (1898) 1–39.
[66] Y.S. Ho, G. McKay, The sorption of lead(II) ions on peat, Water Res., 33 (1999) 578–584.
[67] Y.S. Ho, G. Mckay, The kinetics of sorption of divalent metal ions onto sphagnum moss peat, Water Res., 34 (2000) 735–742.
[68] W.J. Weber, J.C. Morris, Kinetics of adsorption on carbon from solution, J. Sanit. Eng. Div., 89 (1963) 31–60.
[69] A.E. Nemr, Potential of pomegranate husk carbon for Cr(VI) removal from wastewater: kinetic and isotherm studies, J. Hazard. Mater., 161 (2009) 132–141.
[70] D.P. Dutta, S. Nath, Low cost synthesis of SiO_2/C nanocomposite from corn cobs and its adsorption of uranium(VI), chromium(VI) and cationic dyes from wastewater, J. Mol. Liq., 269 (2018) 140–151.
[71] A.E. Kasem, E.A. Abdel-Galil, N. Belacy, N.A. Badawy, Kinetics and adsorption equilibrium of some radionuclides on polyaniline/SiO_2 composite, Radiochim. Acta, 109 (2021) 85–97.
[72] M. Tuzen, A. Sarı, T.A. Saleh, Synthesis, characterization and evaluation of carbon nanofiber modified-polymer for ultra-removal of thorium ions from aquatic media, Chem. Eng. Res. Des., 163 (2020) 76–84.
[73] A.A. El-Sayed, M.M. Hamed, S.A. El-Reefy, Determination of micro-amounts of zirconium in mixed aqueous organic medium by normal and first-derivative spectrophotometry, J. Anal. Chem., 65 (2010) 1113–1117.
[74] M.M. Hamed, Sorbent extraction behavior of a nonionic surfactant, Triton X-100, onto commercial charcoal from low level radioactive waste, J. Radioanal. Nucl. Chem., 302 (2014) 303–313.